Title

- Human class B1 GPCR modulation by plasma membrane lipids.
- Class B1 GPCR interactions with regulatory lipids.

Authors

Kin W Chao,[1,2]† Linda Wong[3], Affiong I Oqua[3], Jas Kalayan[2], Yusman Manchanda[3], James Gebbie-Rayet[2], George Hedger[1,]*, Alejandra Tomas[3,]*, Sarah L Rouse[1,]*

Affiliations

[1] Department of Life Sciences,
Sir Ernst Chain Building,
Imperial College London,
London,
SW7 2AZ,
UK.

[2] Scientific Computing Department,
Science and Technology Facilities Council,
Daresbury Laboratory,
Warrington
WA4 4AD,
UK.

[3] Department of Metabolism, Digestion and Reproduction,
Section of Cell Biology and Functional Genomics,
Imperial College London,
London,
W12 0NN,
UK.

† Present address:

*to whom correspondence should be addressed.
Email: s.rouse@imperial.ac.uk, a.tomas-catala@imperial.ac.uk, g.hedger@imperial.ac.uk.

Abstract

The class B1 G protein-coupled receptor (GPCR) subfamily is a class of receptors known for their regulatory roles in metabolism and neuronal activity important as drug targets. Lipids play key functional roles in modulation of GPCR signalling, yet our understanding of the molecular level detail of specific lipid interactions with class B1 GPCRs remains limited. Here we present coarse-grained molecular dynamics (MD) simulations of the active and inactive states of 15 human class B1 family members and use aiida-gromacs to capture full provenance for the set-up of simulations in complex plasma membranes. Receptors exhibit state-dependent lipid interactions with the regulatory sterol cholesterol and phospholipid phosphatidylinositiol-4,5-bisphosphate [PI(4,5)P_2] at defined locations on the receptor surface. Global analysis of trends across the subfamily reveals conserved patterns of

lipid interaction dynamics. The glycosphingolipid GM3 exerts a modulatory influence on the dynamics of class B1 extracellular domains in both simulations and *in vitro* time-resolved FRET assays.

Teaser

Characterisation of regulatory lipid interactions with all class B1 GPCRs.

MAIN TEXT

Introduction

Class B1 G protein-coupled receptors (GPCRs) are a subfamily of 15 membrane proteins, which are grouped into 5 further subfamilies: Glucagon-like, PTH-like, CT-like, CRF-like and PACAP/VIP-like (*1*) **(**Fig. 1A**)**. These receptors are involved in regulating critical biological processes such as metabolism and neuronal activity and are important drug targets for multiple diseases (*2*). The substrates of class B1 GPCRs are polypeptide hormones, and these receptors are typically characterised by a having a large extracellular domain (ECD) believed to be important in the binding affinity of peptide agonist and signal transduction (*3*). Within the membrane region their structure follows the canonical GPCR seven transmembrane helix bundle. Upon activation, the principal conformational change is the outward movement of the cytoplasmic portion of transmembrane (TM) helix TM6. This exposes a shallow groove with which select G proteins may associate, leading to nucleotide exchange and propagation of signalling to downstream cascades (*4*, *5*).

The plasma membrane environment in which class B1 receptors reside is a key modulator of membrane protein function (*6*, *7*). Several lipid species are reported to have modulatory effects on GPCRs, including cholesterol, phosphatidylinositol-4,5-bisphosphate [PI(4,5)P_2], and the glycosphingolipid GM3 (*8–12*). These modulatory lipids can influence multiple aspects of GPCR function, including the conformational landscape, G protein and arrestin coupling, and oligomerisation state (*13–15*). Such modulation can be brought about by altering the biophysical properties of the local membrane environment, as well as by specific binding of modulatory lipids to allosteric sites on the GPCR (*15*, *16*). Within the class B1 subfamily, cholesterol has been shown to modulate GLP1R signalling responses and biased agonism (*17*). The presence of cholesterol is also required for GLP1R internalisation, optimal receptor clustering and cAMP responses (*18*). However, the molecular level interactions and dynamics which underlie these functional effects and their conservation across the wider subfamily remain obscure.

Recent technological development of cryo-electron microscopy (cryo-EM) approaches (*19*) for GPCR structure determination has led to the elucidation of the active state conformations of all 15 class B1 GPCRs (*20*). However, interpretation of lipid interactions is currently limited due to the use of detergent micelles and non-native lipid compositions within nanodiscs. Likewise, the inactive states of many class B1 GPCRs remain unresolved. In the present study, we leverage advances in simulation methodology (*21*), experimental lipidomics (*22*), and GPU computing (*23*), to reunite experimentally determined structures with their complex plasma membrane environment using large-scale physics-based MD simulations across the entire subfamily. We further leverage recent advances in protein structure prediction models (*24*, *25*) to interrogate the lipid interactions of the predicted inactive states.

During the writing of this manuscript, a new AI foundation model, Chai-1, emerged, which enables the prediction of small molecules in complex with a given protein with AF3-like accuracy (*26*). We applied Chai-1 to predict GPCR-cholesterol, and GPCR-PI(4,5)P_2 complexes, and integrated our findings with the results of physics-based MD simulations. Overall, we identify a conserved pattern of PI(4,5)P_2 binding at the functionally important TM6/7-H8 interface, a number of deep cholesterol binding sites, and GM3 modulation of ECD dynamics, supported by *in vitro* time resolved FRET assays.

Results

We simulated each receptor in a model plasma membrane environment, using the Martini 3 coarse grained force field. We generated active and inactive state models of each class B1 receptor. Available experimental structures of each receptor are shown in Fig. 1A and summarised in Table S1. Each simulation was performed in triplicate for 10 μs, totalling approximately 1.0 ms simulation time.

The vast array of methods and tools used to setup initial atomic configurations and compositions has resulted in complications in capturing protocols used in biomolecular simulations (*27*). With scientific research methodologies focused on *why* and *what* was done to produce simulations, the *how* is often missing, which causes difficulties in reproducing and extending research. Our study uses over 30 different simulation setups with over 60 independent trajectories to analyse, necessitating novel approaches to capture full provenance. Here we present the first application of aiida-gromacs to capture all the metadata associated with this study to allow complete MD provenance including the simulation workflow and analysis (Fig. 1B). The AiiDA python framework (*28*) extensively used in first-principle calculations in computational chemistry, provides a powerful framework for describing the flow of data and enabling the reproduction of complex scientific workflows. The aiida-gromacs plugin (https://aiida-gromacs.readthedocs.io) extends AiiDA to enable the capture and description of biomolecular MD simulations using the GROMACS package. By providing all the metadata as well as the production trajectories, we aim to facilitate greater accessibility to our simulations, towards enabling reproducibility and machine learning approaches.

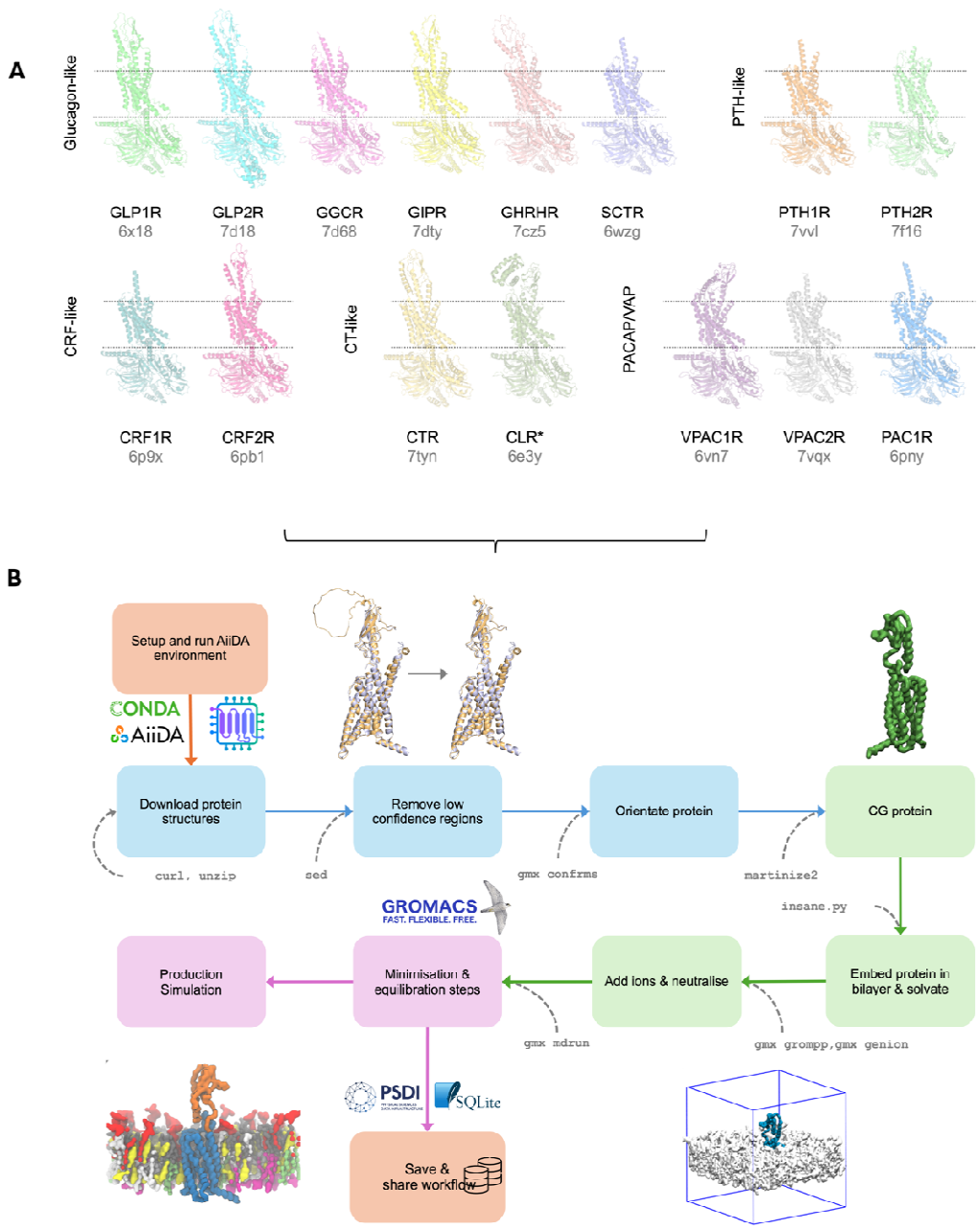

<u>Fig. 1. Modelling and simulation workflow for class B1 GPCRs.</u> (**A**) Structures of the 15 class B1 GPCRs in the active state used here with associated PDB accession codes. For CLR, the structure of CGRP used as the template in GPCRdb is shown. The approximate position in the membrane is shown by dotted lines. (**B**) Schematic of the B1 GPCR simulation workflow steps captured using aiida-gromacs. Orange boxes represent steps involved in enabling provenance capture and sharing, blue boxes represent steps for processing the protein structure, green boxes represent parametrisation and building of the molecular system, and purple boxes represent MD simulation steps. The CLI tools used in each workflow step are shown in grey text.

Broad trends in cholesterol, GM3 and PI(4,5)P_2 interactions for class B1 GPCRs

We observe several trends across the class B1 receptors when comparing cholesterol, GM3 and PI(4,5)P_2 lipid residence time, binding site occupancy, and membrane contact properties of each receptor in active *versus* inactive states (Fig. 2A-C). We also map the occupancy and binding site profile for the active and inactive states (cholesterol, GM3, and PI(4,5)P_2) for each receptor onto their respective sequences using the PyLipID (*29*) package **(**Fig. S1-S3**).**

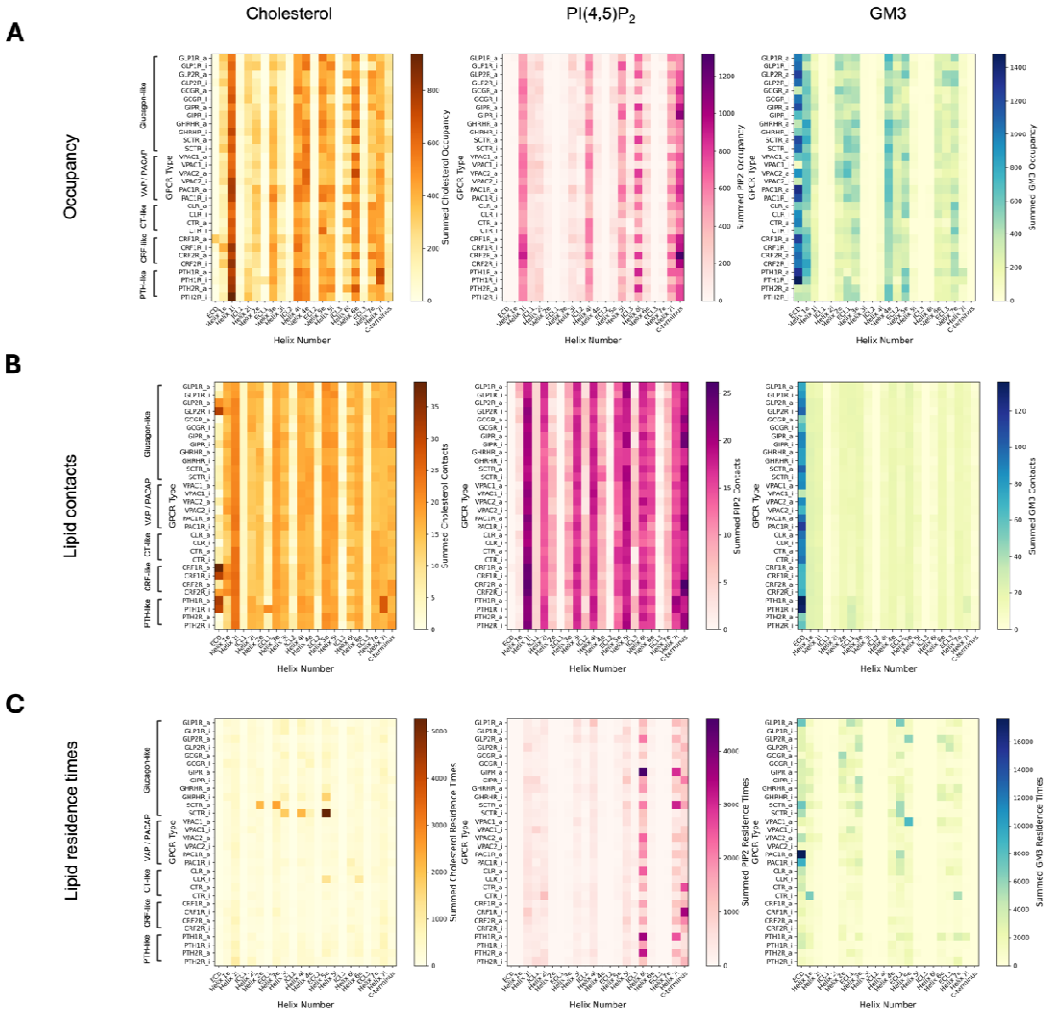

<u>Fig. 2. Global analysis of class B1 GPCR interactions with the regulatory lipids cholesterol, PI(4,5)P_2 and GM3.</u> Lipid occupancy (**A**), lipid contact (**B**) and lipid residence time (**C**) is shown for each class B1 GPCR as a function of ECD, helix, and loop number. Helix 1e denotes the extracellular half of Helix 1, and Helix 1i the intracellular half. Active states are denoted by _a, and inactive by _i. Per residue lipid occupancies were computed using PyLipID (*29*) and summed over the constituent residues of each region. Occupancies were computed over 3 x 9.8 µs of production run simulation time. The residue ranges defining each region correspond to those from GPCRdb (*30*).

All receptors show interactions with cholesterol, PI(4,5)P_2 and GM3, with each lipid exhibiting distinct interaction fingerprints with defined regions of the receptors. Within the inner leaflet of the membrane, the most pronounced changes between active and inactive states for cholesterol and PI(4,5)P_2 contacts occur in the functionally critical TM6 region, which undergoes an outward movement upon activation. In contrast, GM3 interactions show no apparent patterns between inactive and active states, with ECDs of both states contacting GM3 to differing degrees. Binding sites based on occupancy are observed for cholesterol (TM1), PI(4,5)P_2 (TM6/7-H8), and GM3 (ECD). The overall residence times are observed to be in the order GM3 > PI(4,5)P_2 > cholesterol, whilst lipid occupancy is GM3 ~ PI(4,5)P_2 > cholesterol.

As well as capturing the overall patterns of lipid interactions across the B1 receptors, these overview plots allow us to highlight multiple outliers to characterise further. We explore these properties in further detail in the following sections.

Putative novel cholesterol binding sites for class B1 GPCRs

We analysed the top predicted cholesterol binding sites in terms of residence time and occupancy (Fig. S4, S5). Several class B1 receptor structures have been resolved in the presence of cholesterol hemisuccinate, with cholesterol modelled into the map density (*31–37*) (Fig. 3A). Across these, a single cholesterol binding site is conserved at TM4, with the conserved residue $W^{4.50}$, using the Wootten numbering scheme (*38*), proposed to mediate this interaction (*36, 37*). A plot of the cholesterol occupancy mapped onto the aligned sequences indicates that the $W^{4.50}$ interaction is conserved during our simulations (Fig. 3B, Fig. S1). An analysis of all cholesterol headgroup positions mapped to the receptor TM bundle shows that these poses are sampled during our simulations (Fig. 3C). However, the top cholesterol sites defined in terms of occupancy and residence time corresponded to different receptor binding sites (Fig. S4, S5).

Approximately half of the top cgMD sites in active and inactive receptor states correspond to the polar hydroxyl group of cholesterol binding in the center of the membrane, with one or more such sites existing for every receptor (Fig. S4). This “deep membrane” binding mode of cholesterol (*39*), with cholesterol perpendicular to the membrane and its hydroxyl group buried between two TM, has been previously observed in several GPCR simulation studies (*39–42*) but to our knowledge has not been captured in X-ray crystallography or cryo-EM structures of any GPCR to date, although NMR approaches have determined different affinity cholesterol binding sites (*43*). We also observe deep membrane binding modes where the sterol groups of the cholesterol are packed against the TM bundle (Fig. S4).

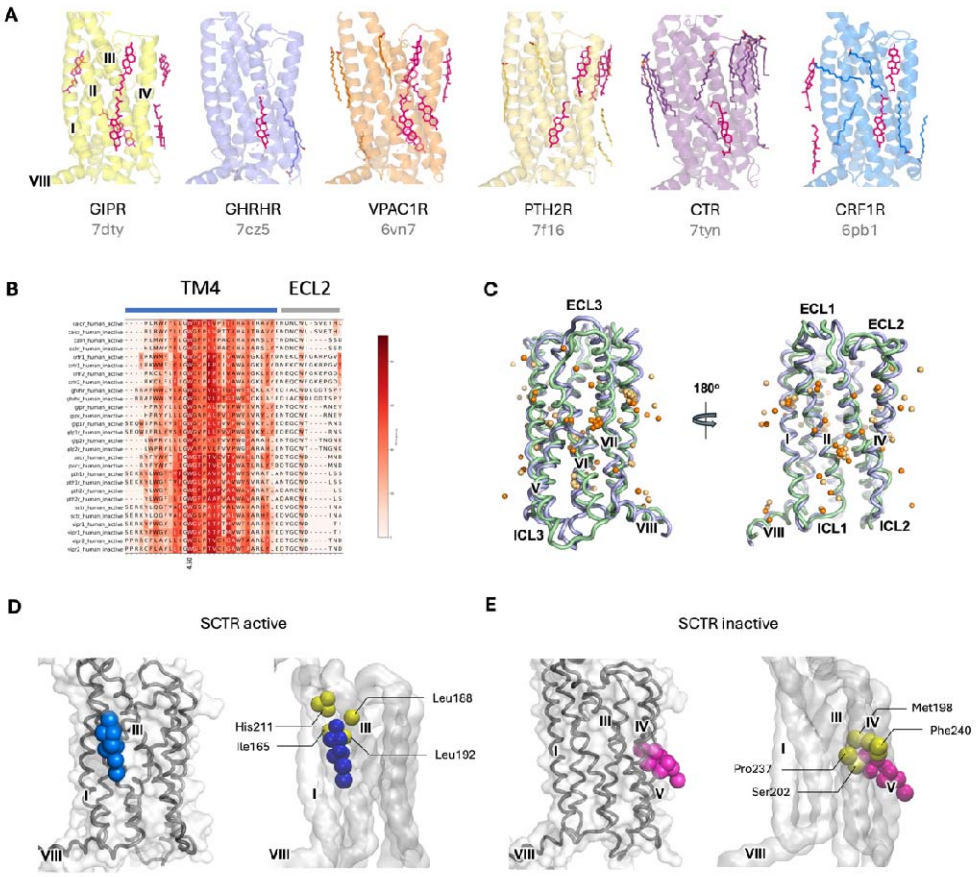

Fig. 3. Cholesterol interactions with class B1 GPCRs. (**A**) Published experimental structures of class B1 receptors containing resolved cholesterol molecules. Structures of the TM regions are aligned, with helix labels shown for GIPR. Cholesterol and cholesterol analogue molecules are shown in magenta stick representation. (**B**) Cholesterol occupancy from cgMD simulations mapped onto sequence alignment across all 15 receptors. (**C**) Positions of cholesterol molecules from simulations mapped onto the CTR receptor. Active (green) and inactive (blue) states of the CTR are shown as a backbone trace. Spheres represent hydroxyl headgroups of cholesterol for the top ranked interaction sites extracted from simulations of active (dark orange) and inactive (light orange) states of all 15 class B1 GPCRs. (**D**) The highest residence time cholesterol site from cgMD simulations for SCTR in the active state, with residues within 6 Å of the cholesterol hydroxyl group shown as yellow spheres. (**E**) As (D) for the SCTR inactive state.

We used a recently released multi-modal foundation model AI, Chai-1 (*26*), to predict cholesterol-receptor complexes across all 15 class proteins (Fig. S6). This predicted the conserved TM4 site with most other predicted sites corresponding to those observed in the cryo-EM structures (Fig. 3A). No cholesterol deep membrane binding modes were observed. This likely reflects the model training, which is in part based on PDB X-ray and cryo-EM structures, which may be considered to contain a 'biased sample' of tight binding lipids (*44*). That is, those which bind tightly enough to survive the purification, detergents, and non-native temperatures (*45*) used during

structure determination. The dynamic 'greasy patch' binding of cholesterol molecules we observe in MD simulations, and particularly deep membrane cholesterol, is likely to be challenging to resolve by these methods.

A comparison of the cholesterol site residence times across the class B1 GPCRs highlights a clear outlier in the case of the secretin receptor (SCTR, Fig. 2A), which contained an up to 10-fold higher affinity binding site in both the active (692 ns) and inactive (1854 ns) states than any other class B1 receptor in these simulations (maximum residence time range for other receptors was 50 – 255 ns active, 72 – 170 ns inactive). When compared to the active state cryo-EM structure, we observe a shift in the position of His211 in the ECL1 loop during the simulation, which forms a contact with the cholesterol hydroxyl group in the active state (Fig. 3D). For the inactive state, the cholesterol adopts a deep membrane binding mode and buries into the gap between TM4 and TM5 (Fig. 3E) The key residues responsible for mediating the contacts in both sites are shown in Figure 3ED. The Chai-1 prediction does not resolve this pose (Fig. S7), likely due to the model plasma membrane environment being required for the conformational change of His211.

Conserved PI(4,5)P_2 interactions at TM6/7 and H8

The inner leaflet lipid PI(4,5)P_2 interacted with all class B1 receptors with maximum residence times in the range 955 – 6455 ns (active) and 216 to 1273 ns (inactive) (Fig. 4A). These interactions were concentrated at the intracellular tips of TM6/7, and either side of H8 (Fig. S3). For all receptors, PI(4,5)P_2 interactions at the TM6/7 site showed enhanced stability in simulations of the active state compared to the inactive state (Fig. S3, S8). This site was also predicted by Chai-1, along with a second site between TM2/4 (Fig. 4A). Analysis of the degree of direct contact that each residue formed with PI(4,5)P_2 during simulations exhibited a similar trend, with increased levels of per residue contact in the active state (Fig. S3). We analysed the top active and inactive state site for GIPR which showed one of the highest residence times for PI(4,5)P_2 in the active state in our simulations (Fig. 4C, 4D). Particularly high levels of interaction were seen between basic residues and the anionic 4' and 5' phosphoryl moieties of the PI(4,5)P_2 headgroup. These residues are highly conserved across class B1 GPCRs (Fig. 4B). Binding of PI(4,5)P_2 lipids was also seen on the opposing side of H8, adjacent to TM1. Binding at this location is similarly driven by contact with basic residues in H8 and the adjacent TM1 (Fig. 4D).

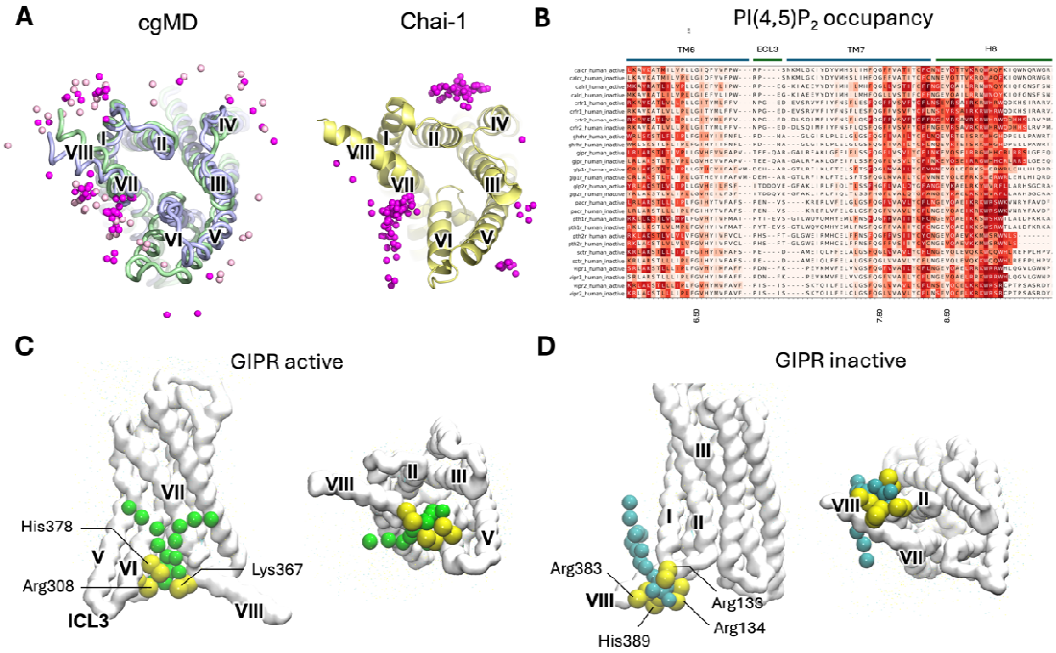

Fig. 4. Interactions of PI(4,5)P_2 with class B1 GPCRs. (**A**) Alignment of top ranked PyLipID PI(4,5)P_2 interaction sites across all 15 receptors from cgMD simulation and Chai-1. The view shown is from the cytoplasmic side onto the base of the active (green) and inactive (blue) states of the CTR. Spheres represent PI(4,5)P_2 headgroups for the top ranked interaction sites extracted from simulations of active (dark magenta) and inactive (light pink) states of all 15 class B1 GPCRs. Chai-1 predicted an active state for all 15 receptors. For each receptor, five Chai-1 models were generated, each containing three PI(4,5)P_2 poses. This yielded 15 poses per receptor, and 225 poses overall. Only poses within the inner leaflet were considered. (**C**) Highest residence time PI(4,5)P_2 site in the GIPR active state corresponding to TM6/7, and H8. Residues in contact with the PI(4,5)P_2 are labelled. (**D**) Highest residence time PI(4,5)P_2 binding site in the inactive GIPR receptor, with residues in contact with the lipid headgroup shown .

The glycosphingolipid GM3 modulates the mobility of receptor ECDs

To characterise the interactions of ECDs with the plasma membrane, we analysed the ECD mobility of each GPCR in each state relative to the TM bundle (Fig. SI9). Results demonstrate that all B1 receptors in inactive and active states exhibit some degree of mobility of the ECD, but some receptors sample a much larger conformational space: GIPR, CRF1R and GHRHR (active states), and PAC1R, PTH1R and GLP2R (both states) showed the greatest mobility in our cgMD simulations.

To define the role of GM3 in ECD mobility, we chose to focus on two receptors in detail: GIPR, which showed the widest conformational variability in these simulations, and GLP1R which is representative of the overall B1 receptors, showing moderate mobility during our simulations (Fig. 5A, 5E). For the GLP1R and GIPR, we observed different modes of GM3 binding. For the active state GLP1R, GM3

bound tightly (maximum residence time 1525 ns) to the base of the ECD and the orthosteric ligand pocket, restricting the mobility of this domain (Fig. 5B). For the inactive state GLP1R, GM3 bound to the base of the ECD but did not interact with the orthosteric pocket, with a maximum residence time of 398 ns. For GIPR, GM3 was found to bind to the distal end of the ECD, forming contacts from the bulk membrane, with maximum residence times of 590 nsfor the active state, and 718 nsfor the inactive state (Fig. 5F).

To further assess the role of GM3 in ECD modulation, we ran comparative cgMD simulations with GM3 absent from the membrane. To quantify the ECD motion, we calculated the ECD bend angle (*12*) relative to the TM bundle (Fig. S10) for each state, with and without GM3 present in the membrane (Fig. 5C, 5G). For active state GLP1R, the absence of GM3 caused a small shift in the position of the ECD relative to the TM domain. For active state GIPR, a pronounced difference was observed, with the presence of GM3 restricting the motion of the ECD such that it remained membrane interacting (Fig. 5F, 5G). The inactive state remained highly flexible with and without GM3, able to contact the membrane by forming two different states (Fig. 5F).

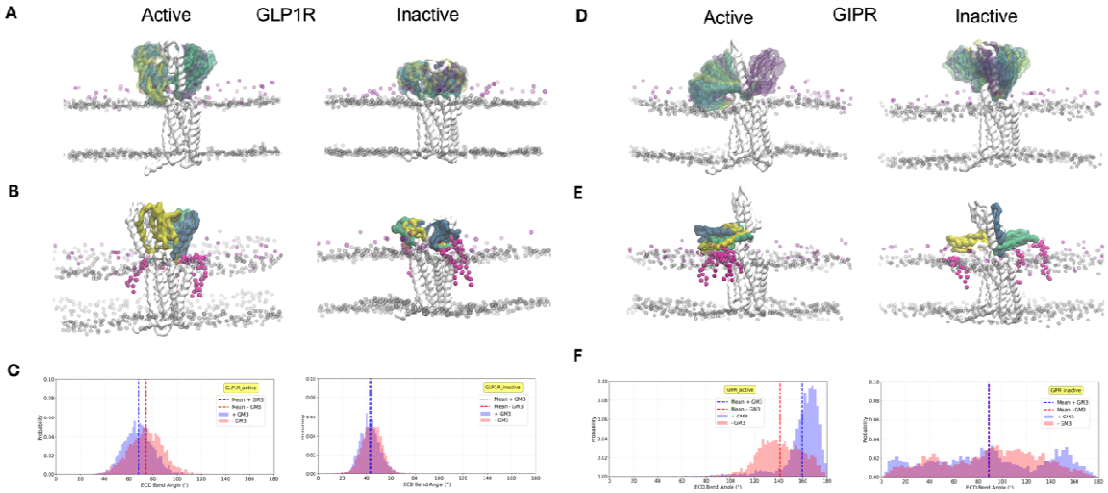

<u>Figure 5. Modulation of GLP1R and GIPR ECDs by GM3 in cgMD simulations.</u> (**A**) Motion of the ECD during 10 µs simulation time for the active and inactive states for GLP1R. The starting structure is shown as solid grey, whilst the ECD motion relative to the TM bundle is shown coloured by timestep (0 to 10 µs, blue-green-yellow). Phospholipid headgroup beads are shown as transparent grey spheres and GM3 GL beads are shown in magenta. (**B**) Final 10 µs conformations for each repeat. GM3 lipids within 6 Å of the ECD backbone are shown in magenta for the final frame of the first repeat. (**C**) Histogram of the angle between the ECD and the TM bundle for the simulations with GM3 present. (**D**) ECD motion of GIPR during simulation, coloured as in (A). (**E**) GIPR final conformations for each run, with all GM3 lipids contacting the ECD in the final frames shown, coloured as in (B). (**F**) Histogram of ECD angles for GIPR, as described in (C).

To experimentally validate the observed role of GM3 in modulation of the ECD of GLP1R and GIPR in our simulations, we used a time-resolved Förster resonance

energy transfer (TR-FRET) assay to measure receptor ECD proximity to the plasma membrane under vehicle and stimulated conditions (Fig. 6A). Experiments were conducted in the presence and absence of the glucocerebroside synthase inhibitor Eliglustatto inhibit GM3 synthesis (*46*). For GLP1R, stimulation with the agonist exendin-4 elicited a conformational rearrangement resulting in increased TR-FRET between the receptor ECD and the plasma membrane, an effect that we interpret as a proxy for ECD opening upon agonist binding. Additionally, a significant reduction in ECD opening was observed in the presence of Eliglustat , indicating that the ECD of GLP1R is more flexible when there is GM3 in the plasma membrane (Fig. 6B). Conversely, for GIPR, we observed that the ECD was less dynamic in the active (GIP-stimulated) compared to the inactive state(Fig. 6C), potentially due to the membrane-bound ECD open-state mode observed during the cgMD simulations. No significant difference in ECD opening between the untreated and the Eliglustat-treated conditions was observed for GIPR. Moreover, a higher basal state fluorescence indicated that the GIPR ECD is interacting with the membrane in the basal state more than GLP1R, consistent with our simulations (Fig. 5F). Taking the simulation and experimental results together, this suggests that a fully closed inactive state, observed in the cryo-EM structure of GLP1R, may not exist for GIPR.

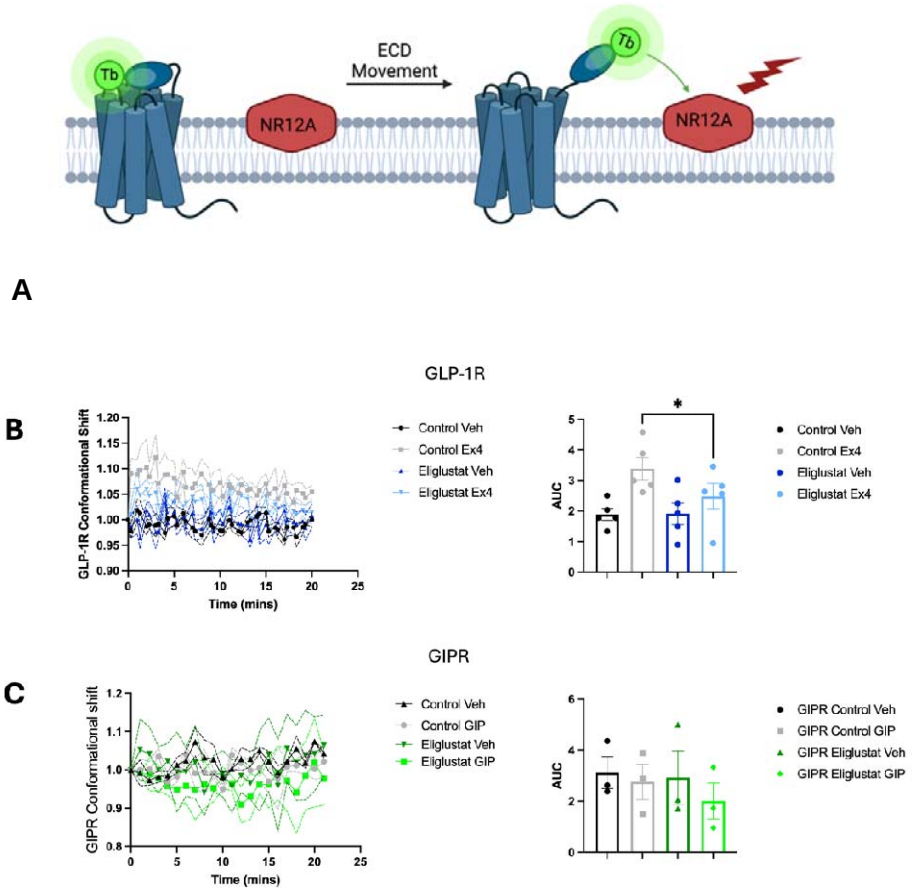

Fig. 6. TR-FRET ECD opening conformational shift assay. (**A**) Schematic diagram showing the ECD – plasma membrane conformational shift assay: SNAP-tagged receptors are expressed in pancreatic β-cells to mimic native plasma membrane lipid composition, followed by Terbium (LumiTb, Tb) labelling of the SNAP-tag and NR12A labelling of the plasma membrane prior to TR-FRET analysis. (**B**, **left**) Conformational shift response (TR-FRET ratio) over time between SNAP-Lumi4Tb-labelled GLP1R and NR12A under Control or 300 μM Eliglustat conditions following stimulation with vehicle (Veh) or 100 nM exendin-4 (Ex4); (**B**, **right**) Area under the curve (AUC) for the TR-FRET kinetic response; n = 5. (**C**, **left**) Conformational shift response (TR-FRET ratio) over time between SNAP-Lumi4Tb-labelled GIPR and NR12A under Control or 300 μM Eliglustat conditions following stimulation with vehicle (Veh) or 100 nM GIP; (**C**, **right**) Area under the curve (AUC) for the TR-FRET kinetic response; n = 3.

Discussion

This study of class B1 GPCRs has identified trends in specific lipid interactions across the subfamily, highlighting avenues for further in-depth exploration. Key areas include the "deep membrane" binding mode of cholesterol which has been observed in multiple simulation studies at both coarse grained and atomistic resolution, but to the best of our knowledge has not been captured by experimental methods. Our previous work on GLP1R has provided evidence that mutating a cholesterol binding site impacts downstream signalling and functional responses (*17*). The results presented here indicate that the secretin receptor may be more tightly modulated by cholesterol, with distinct high residence time cholesterol binding sites in the active and inactive states potentially indicating a route to modulating biased signalling of this receptor. The His211 identified in the long residence time active state site and the Ser202 of the inactive state site are shown in the gnomAD database (*47*) as variants of potential interest, with unknown pathogenicity.

We found that, in a model plasma membrane, class B1 ECDs are highly mobile. Our analysis of GM3 ECD modulation of GLP1R and GIPR by both simulation and experiment demonstrate that GM3 has receptor-specific effects on ECD modulation, adding to the growing body of evidence that GM3 influences GPCR behaviour. Previous studies have shown that both GCGR and GHRHR are modulated by GM3. The present study indicates that this is a general feature of the class B1 GPCRs and may be a valuable pathway to explore for future therapeutic design efforts.

We additionally identify a highly conserved PI(4,5)P_2 interaction site formed by TM6/7 and H8 *via* physics-based simulation. PI(4,5)P_2 binding at this site shows a strong preference for the active over the inactive state, with the outward movement of TM6 exposing additional surface area and residues, as well as a 'groove-like' architecture into which a PI(4,5)P_2 lipid may 'slot'. This site has previously been reported for isolated studies of the glucagon receptor (GCGR) (*12*, *48*). The markedly high degree of conservation that we observe across all B1 receptors, the strength of interaction, and the location of this site adjacent to TM6, which undergoes the key movement seen during the inactive/active conformational change, is particularly intriguing. This raises the prospect that PI(4,5)P_2 may modulate the kinetics of the transition and/or stabilise the active state, as has been seen for select class A GPCRs (*49*, *50*). Similarly, binding of PI(4,5)P_2 at this site in class B1 GPCRs may have a role in the recruitment of soluble intracellular signalling partners. In class A GPCRs,

$PI(4,5)P_2$ binding at TM4 and TM1 has been shown to stabilise the active state, and enhance coupling to mini-$G\alpha_s$ over mini-$G\alpha_i$ and mini-$G\alpha_{12}$ by acting as a 'molecular glue' to bridge complex formation (*16*). Functional experiments have also reported a role of $PI(4,5)P_2$ in enhancing β-arrestin recruitment for select GPCRs (*11*, *42*, *51*, *52*). The $PI(4,5)P_2$ site identified in the present study of class B1 GPCRs is particularly conserved across the subfamily compared to $PI(4,5)P_2$ sites in class A GPCRs (*16*, *42*), and merits further investigation as to its possible functional consequences. We note that two antagonists of the GCGR have been resolved bound at this same interaction site (PDB ids: 5EE7 and 5XEZ) (*53*, *54*), raising the prospect of direct phosphoinositide / drug competition and synergistic binding effects. Similarly, a positive allosteric modulator (PAM) used to stabilise structures of GIPR in complex with the antidiabetic therapeutic tirzepatide (Mounjaro) (PDB id: 7RBT) binds proximal to the TM6/7-H8 site and may interact with lipids in this site (*55*).

Taken together, our comparison of cgMD simulations to the artificial intelligence-based predictions shows that interactions requiring model membrane environments or subtle conformational changes are not yet captured by structure prediction-based approaches, highlighting that the molecular simulation approaches remain a powerful tool in studies of membrane protein-lipid interactions. Tools such as aiida-gromacs, alongside efforts to standardise data in the simulation field, including MDVerse (*56*)and the Molecular Dynamics Data Bank (https://mddbr.eu), may enable training of AI models and improve predictive capacity within complex bilayer environments.

Limitations

It is important to discuss the limitations of the present study. Our study was enabled by the availability of all 15 receptor cryo-EM structures, but these were mostly in the monomeric active state, whilst most inactive states had no experimental structures available. There is therefore a need for further class B1 GPCR structural studies. We used the Martini 3 forcefield which has been extensively employed for specific protein-lipid interactions. This has the advantage of stabilising inactive states in substrate and G protein-free conformation, but with the consequence that it limits the conformational space explored.

There are multiple routes to extend this work, including experiments to validate the novel cholesterol and $PI(4,5)P_2$ binding sites described here, as well as confirming the family-wide modulation of the ECDs by GM3. We have made our set up and simulation files available to the community to build on this study. Future work will lead to building a more complete picture of class B1 GPCR signalling, by including heterodimerisation states (*57*), substrates, G protein/ β-arrestin complexes and post translational modifications (*58*).

Materials and Methods

GPCR Model Building

B1 GPCRs structures in active and inactive states were taken from cryo-electron microscopy (cryo-EM) structures and AlphaFold multistate models deposited in GPCRdb (*59*). For the inactive state, the GPCRdb models were used when there were no experimental structures available (13/15 inactive states). For active state structures, GPCRdb models were used for consistency when the Cα RMSD with the

experimental structure was < 0.8 Å. Above this cut off the ECD in GPCRdb models did not align with the experimental structure, and so the ECD from the experimental structure was used instead (Table S1). The low-confidence region in the N-terminal ECD and C-terminal tail were removed to match the existing experimental structures for all GPCRdb models used. Modeller v10.1 (*60*) was used to add missing loops and the CHARMM-GUI PDB reader (*61*) was used to model any missing atoms in experimental structures. All models used in this study used the native human sequence. Further information about each model, along with the associated PDB accession codes (*62*) and references can be found in Table S1.

Coarse-grained MD Simulations

GPCR structures were converted to a coarse-grained representation using Martinize2 (*63*) and the Martini 3 force field (*21*). ElNeDyn elastic network restraints were applied to each GPCR using an elastic bond force constant of 500 kJ/mol/nm^2 and an upper cut-off of 0.9 nm (*64*). The transmembrane region of GPCR was predicted using PPM 3.0 Web Server (*65*) and embedded into an asymmetric lipid membrane bilayer in a 25 x 25 x 19 nm^3 box using the insane script (*66*). The mammalian plasma membrane composition previously described (*67*) was used as follows: POPC (25%), DOPC (25%), POPE (8%), DOPE (7%), GM3 (10%) and cholesterol (25%) in the upper leaflet, and POPC (5%), DOPC (5%), POPE (20%), DOPE (20%), POPS (8%), DOPS (7%), POPI(4,5)P_2 (10%) and cholesterol (25%). For the simulations of GLP1R and GIPR in a 0% GM3 membrane, POPC and DOPC were increased to 30% each in the upper leaflet with all other components the same. The most recent Martini 3 parameters for PI(4,5)P_2 (*68*) and cholesterol (*69*) were used. Each system was solvated using Martini water (*21*) and 0.15 M NaCl followed by minimisation and equilibration steps using protocol files from CHARMM-GUI Martini Maker (*70*). Briefly, the system was subjected to steepest descents energy minimisation, followed by six sequential NPT equilibration steps with restraints with decreasing force constant in each subsequent step from 1000 kJ/(mol nm^2) to 50 kJ/(mol nm^2) for the protein backbone and 200 kJ/(mol nm^2) to 10 kJ/(mol nm^2) for lipid headgroups.

Production run simulations were performed for 10 μs of cgMD. Three repeats were run for each active and inactive state, initiated from the same initial particle configurations, and random initial velocity seeds. A summary of simulations performed can be found in Table 1. The v-rescale thermostat (tau 1.0 ps) (*71*) and the Parrinello–Rahman barostat (tau 12.0 ps) (*72*) were used to maintain temperature (303.15 K) and pressure (1 bar) on all production runs. All simulations were performed using GROMACS 2022.4 (https://doi.org/10.5281/zenodo.7323393). Lipid interaction profiles were calculated using PyLipID (*29*) with a cut-off of 0.7 nm to calculate lipid residence time and occupancy profiles across all three repeats. VMD (*73*) and PyMOL (*74*) was used for trajectory visualisation and analysis.

Reproducible simulation protocols with aiida-gromacs

These simulations were produced using an automated workflow with each step for setting up the system captured using aiida-gromacs, allowing others to reuse or extend our dataset to more GPCRs. An exemplar trajectory and starting files are available on zenodo along with the single AiiDA archive file, which contains all the steps involved to reproduce the simulation methodology described above. Along with the raw files

and simulation metadata, a Jupyter Notebook tutorial (https://github.com/PSDI-UK/aiida-gromacs/tree/master/notebooks, https://aiida-gromacs.readthedocs.io/en/latest/tutorials/PTH2R_CGMD.html) is available, showcasing the simplicity in provenance capture using aiida-gromacs in this study.

AI models

The AI models generated for this study utilized the Chai-1 multi-modal foundation model described in (*26*)(https://github.com/chaidiscovery/chai-lab/). Models were generated using the web interface (https://lab.chaidiscovery.com/), with the multiple sequence alignment (MSA) option active for enhanced accuracy. The model we utilized had a training cutoff date of 2021-01-12 and will not have seen experimental GPCR-cholesterol structures after this date. Primary sequences of the same class B1 constructs used in MD simulations were extracted and used as input for the Chai-1 model, along with the SMILES strings for cholesterol, and PI(4,5)P_2. SMILES strings were obtained from PubChem (*75*). The PI(4,5)P_2 variant used was the 1-stearoyl-2-arachidonoyl, which is the most common tail saturation pattern for PI(4,5)P_2 in human cells (*76*). Five AI models were generated for each cholesterol run, with three cholesterol molecules in each run. This yielded a total of 15 cholesterol poses for each receptor, and 225 cholesterol poses globally across all receptors. PI(4,5)P_2 predictions followed the same protocol.

Conformational Assay by TR-FRET

INS-1 832/3 pancreatic β-cells stably expressing SNAP/FLAG-hGLP1R or SNAP/FLAG-hGIPR were pre-incubated in suspension with 40 nM of SNAP-Lumi4-Tb (SSNPTBC, Cisbio), a lanthanide fluorophore probe for TR-FRET, or 40 nM SNAP-Lumi4Tb plus 300 µM Eliglustat, an inhibitor of GM3 gangliosides(*77*) for 1 hour at 37°C in full culture media. Cells were pelleted and washed with HBSS and then resuspended in 100 nM NR12A, a Nile red-based plasma membrane fluorescent probe (*78*), diluted in HBSS, incubated for 5 minutes, and then seeded unto white opaque 96-well half-area plates. TR-FRET was carried out as previously described (*79*). Briefly, a baseline reading was taken for 5 minutes using a Flexstation 3 plate reader with an excitation of 335 nm, emission of 490 nm and 590 nm at 37°C. The cells were stimulated with vehicle or either 100 nM Exendin-4 (GLP1R) or 100 nM GIP (GIPR) and the plate was read for a further 20 minutes at 37°C. Receptor conformational shift was calculated as the ratio of the fluorescent signal of both wavelengths (590/490 nm) after normalising to basal signal. AUC was calculated and used for statistical analysis.

References

1. Z. Cong, Y. L. Liang, Q. Zhou, S. Darbalaei, F. Zhao, W. Feng, L. Zhao, H. E. Xu, D. Yang, M. W. Wang, Structural perspective of class B1 GPCR signaling. [Preprint] (2022). https://doi.org/10.1016/j.tips.2022.01.002.
2. V. Karageorgos, M. Venihaki, S. Sakellaris, M. Pardalos, G. Kontakis, M. T. Matsoukas, A. Gravanis, A. Margioris, G. Liapakis, Current understanding of the structure and function of family B GPCRs to design novel drugs. [Preprint] (2018). https://doi.org/10.1007/s42000-018-0009-5.
3. B. P. Cary, X. Zhang, J. Cao, R. M. Johnson, S. J. Piper, E. J. Gerrard, D. Wootten, P. M. Sexton, New Insights into the Structure and Function of Class B1 GPCRs. [Preprint] (2023). https://doi.org/10.1210/endrev/bnac033.
4. N. R. Latorraca, A. J. Venkatakrishnan, R. O. Dror, GPCR dynamics: Structures in motion. [Preprint] (2017). https://doi.org/10.1021/acs.chemrev.6b00177.

5. A. S. Hauser, A. J. Kooistra, C. Munk, F. M. Heydenreich, D. B. Veprintsev, M. Bouvier, M. M. Babu, D. E. Gloriam, GPCR activation mechanisms across classes and macro/microscales. *Nat Struct Mol Biol* **28** (2021).
6. A. Laganowsky, E. Reading, T. M. Allison, M. B. Ulmschneider, M. T. Degiacomi, A. J. Baldwin, C. V Robinson, Membrane proteins bind lipids selectively to modulate their structure and function. *Nature* **510**, 172–5 (2014).
7. P. L. Yeagle, Non-covalent binding of membrane lipids to membrane proteins. [Preprint] (2014). https://doi.org/10.1016/j.bbamem.2013.11.009.
8. E. F. X. Byrne, R. Sircar, P. S. Miller, G. Hedger, G. Luchetti, S. Nachtergaele, M. D. Tully, L. Mydock-Mcgrane, D. F. Covey, R. P. Rambo, M. S. P. Sansom, S. Newstead, R. Rohatgi, C. Siebold, Structural basis of Smoothened regulation by its extracellular domains. *Nature* **535** (2016).
9. J. Oates, A. Watts, Uncovering the intimate relationship between lipids, cholesterol and GPCR activation. [Preprint] (2011). https://doi.org/10.1016/j.sbi.2011.09.007.
10. S. Kiriakidi, A. Kolocouris, G. Liapakis, S. Ikram, S. Durdagi, T. Mavromoustakos, "Effects of cholesterol on GPCR function: Insights from computational and experimental studies" in *Advances in Experimental Medicine and Biology* (2019)vol. 1135.
11. J. Janetzko, R. Kise, B. Barsi-Rhyne, D. H. Siepe, F. M. Heydenreich, K. Kawakami, M. Masureel, S. Maeda, K. C. Garcia, M. von Zastrow, A. Inoue, B. K. Kobilka, Membrane phosphoinositides regulate GPCR-β-arrestin complex assembly and dynamics. *Cell* **185** (2022).
12. T. B. Ansell, W. Song, M. S. P. Sansom, The Glycosphingolipid GM3 Modulates Conformational Dynamics of the Glucagon Receptor. *Biophys J* **119** (2020).
13. K. Pluhackova, S. Gahbauer, F. Kranz, T. A. Wassenaar, R. A. Böckmann, Dynamic Cholesterol-Conditioned Dimerization of the G Protein Coupled Chemokine Receptor Type 4. *PLoS Comput Biol* **12** (2016).
14. R. Guixà-González, M. Javanainen, M. Gómez-Soler, B. Cordobilla, J. C. Domingo, F. Sanz, M. Pastor, F. Ciruela, H. Martinez-Seara, J. Selent, Membrane omega-3 fatty acids modulate the oligomerisation kinetics of adenosine A2A and dopamine D2 receptors. *Sci Rep* **6** (2016).
15. R. Dawaliby, C. Trubbia, C. Delporte, M. Masureel, P. Van Antwerpen, B. K. Kobilka, C. Govaerts, Allosteric regulation of G protein-coupled receptor activity by phospholipids. *Nat Chem Biol* **12** (2016).
16. H. Y. Yen, K. K. Hoi, I. Liko, G. Hedger, M. R. Horrell, W. Song, D. Wu, P. Heine, T. Warne, Y. Lee, B. Carpenter, A. Plückthun, C. G. Tate, M. S. P. Sansom, C. V. Robinson, PtdIns(4,5)P2 stabilizes active states of GPCRs and enhances selectivity of G-protein coupling. *Nature* **559** (2018).
17. A. I. Oqua, K. Chao, L. El Eid, L. Casteller, A. Miguéns, S. Barg, B. Jones, J. B. de la Serna, S. L. Rouse, A. Tomas, Molecular mapping and functional validation of GLP-1R cholesterol binding sites in pancreatic beta cells. doi: 10.7554/elife.101011.1 (2024).
18. T. Buenaventura, S. Bitsi, W. E. Laughlin, T. Burgoyne, Z. Lyu, A. I. Oqua, H. Norman, E. R. McGlone, A. S. Klymchenko, I. R. Corrêa, A. Walker, A. Inoue, A. Hanyaloglu, J. Grimes, Z. Koszegi, D. Calebiro, G. A. Rutter, S. R. Bloom, B. Jones, A. Tomas, Agonist-induced membrane nanodomain clustering drives GLP-1 receptor responses in pancreatic beta cells. *PLoS Biol* **17** (2019).
19. Y. Cheng, Membrane protein structural biology in the era of single particle cryo-EM. [Preprint] (2018). https://doi.org/10.1016/j.sbi.2018.08.008.
20. M. Zhang, T. Chen, X. Lu, X. Lan, Z. Chen, S. Lu, G protein-coupled receptors (GPCRs): advances in structures, mechanisms and drug discovery. *Signal Transduct Target Ther* **9**, 88 (2024).
21. P. C. T. Souza, R. Alessandri, J. Barnoud, S. Thallmair, I. Faustino, F. Grünewald, I. Patmanidis, H. Abdizadeh, B. M. H. Bruininks, T. A. Wassenaar, P. C. Kroon, J. Melcr, V. Nieto, V. Corradi, H. M. Khan, J. Domański, M. Javanainen, H. Martinez-Seara, N. Reuter, R. B. Best, I. Vattulainen, L. Monticelli, X. Periole, D. P. Tieleman, A. H. de Vries, S. J. Marrink, Martini 3: a general purpose force field for coarse-grained molecular dynamics. *Nat Methods* **18** (2021).
22. X. Han, R. W. Gross, The foundations and development of lipidomics. [Preprint] (2022). https://doi.org/10.1016/j.jlr.2021.100164.
23. S. Páll, A. Zhmurov, P. Bauer, M. Abraham, M. Lundborg, A. Gray, B. Hess, E. Lindahl, Heterogeneous parallelization and acceleration of molecular dynamics simulations in GROMACS. *Journal of Chemical Physics* **153** (2020).
24. J. Abramson, J. Adler, J. Dunger, R. Evans, T. Green, A. Pritzel, O. Ronneberger, L. Willmore, A. J. Ballard, J. Bambrick, S. W. Bodenstein, D. A. Evans, C.-C. Hung, M. O'Neill, D. Reiman, K. Tunyasuvunakool, Z. Wu, A. Žemgulytė, E. Arvaniti, C. Beattie, O. Bertolli, A. Bridgland, A. Cherepanov, M. Congreve, A. I. Cowen-Rivers, A. Cowie, M. Figurnov, F. B. Fuchs, H. Gladman, R. Jain, Y. A. Khan, C. M. R. Low, K. Perlin, A. Potapenko, P. Savy, S. Singh, A. Stecula, A. Thillaisundaram, C. Tong, S. Yakneen, E. D. Zhong, M. Zielinski, A. Žídek, V. Bapst, P. Kohli, M. Jaderberg, D. Hassabis, J. M. Jumper, Accurate structure prediction of biomolecular interactions with AlphaFold 3. *Nature* **630**, 493–500 (2024).
25. L. Heo, M. Feig, Multi-state modeling of G-protein coupled receptors at experimental accuracy. *Proteins: Structure, Function and Bioinformatics* **90** (2022).

26. C. Discovery, J. Boitreaud, J. Dent, M. McPartlon, J. Meier, V. Reis, A. Rogozhnikov, K. Wu, Chai-1: Decoding the molecular interactions of life. *bioRxiv*, doi: 10.1101/2024.10.10.615955 (2024).
27. T. Bereau, L. J. Walter, J. F. Rudzinski, Martignac: Computational workflows for reproducible, traceable, and composable coarse-grained Martini simulations. [Preprint] (2024). https://arxiv.org/abs/2409.15478.
28. S. P. Huber, S. Zoupanos, M. Uhrin, L. Talirz, L. Kahle, R. Häuselmann, D. Gresch, T. Müller, A. V. Yakutovich, C. W. Andersen, F. F. Ramirez, C. S. Adorf, F. Gargiulo, S. Kumbhar, E. Passaro, C. Johnston, A. Merkys, A. Cepellotti, N. Mounet, N. Marzari, B. Kozinsky, G. Pizzi, AiiDA 1.0, a scalable computational infrastructure for automated reproducible workflows and data provenance. *Sci Data* **7** (2020).
29. W. Song, R. A. Corey, T. B. Ansell, C. K. Cassidy, M. R. Horrell, A. L. Duncan, P. J. Stansfeld, M. S. P. Sansom, PyLipID: A Python Package for Analysis of Protein-Lipid Interactions from Molecular Dynamics Simulations. *J Chem Theory Comput* **18** (2022).
30. G. Pándy-Szekeres, J. Caroli, A. Mamyrbekov, A. A. Kermani, G. M. Keseru, A. J. Kooistra, D. E. Gloriam, GPCRdb in 2023: state-specific structure models using AlphaFold2 and new ligand resources. *Nucleic Acids Res* **51** (2023).
31. X. Wang, X. Cheng, L. Zhao, Y. Wang, C. Ye, X. Zou, A. Dai, Z. Cong, J. Chen, Q. Zhou, T. Xia, H. Jiang, H. E. Xu, D. Yang, M. W. Wang, Molecular insights into differentiated ligand recognition of the human parathyroid hormone receptor 2. *Proc Natl Acad Sci U S A* **118** (2021).
32. J. Duan, D. dan Shen, X. E. Zhou, P. Bi, Q. feng Liu, Y. xia Tan, Y. wen Zhuang, H. bing Zhang, P. yu Xu, S. J. Huang, S. shan Ma, X. heng He, K. Melcher, Y. Zhang, H. E. Xu, Y. Jiang, Cryo-EM structure of an activated VIP1 receptor-G protein complex revealed by a NanoBiT tethering strategy. *Nat Commun* **11** (2020).
33. J. Cao, M. J. Belousoff, Y. L. Liang, R. M. Johnson, T. M. Josephs, M. M. Fletcher, A. Christopoulos, D. L. Hay, R. Danev, D. Wootten, P. M. Sexton, A structural basis for amylin receptor phenotype. *Science (1979)* **375** (2022).
34. F. Zhou, H. Zhang, Z. Cong, L. H. Zhao, Q. Zhou, C. Mao, X. Cheng, D. D. Shen, X. Cai, C. Ma, Y. Wang, A. Dai, Y. Zhou, W. Sun, F. Zhao, S. Zhao, H. Jiang, Y. Jiang, D. Yang, H. Eric Xu, Y. Zhang, M. W. Wang, Structural basis for activation of the growth hormone-releasing hormone receptor. *Nat Commun* **11** (2020).
35. F. Zhao, C. Zhang, Q. Zhou, K. Hang, X. Zou, Y. Chen, F. Wu, Q. Rao, A. Dai, W. Yin, D. D. Shen, Y. Zhang, T. Xia, R. C. Stevens, H. E. Xu, D. Yang, L. Zhao, M. W. Wang, Structural insights into hormone recognition by the human glucosedependent insulinotropic polypeptide receptor. *Elife* **10** (2021).
36. L. H. Zhao, S. Ma, I. Sutkeviciute, D. D. Shen, X. Edward Zhou, P. W. De Waal, C. Y. Li, Y. Kang, L. J. Clark, F. G. Jean-Alphonse, A. D. White, D. Yang, A. Dai, X. Cai, J. Chen, C. Li, Y. Jiang, T. Watanabe, T. J. Gardella, K. Melcher, M. W. Wang, J. P. Vilardaga, H. Eric Xu, Y. Zhang, Structure and dynamics of the active human parathyroid hormone receptor-1. *Science (1979)* **364** (2019).
37. S. Ma, Q. Shen, L. H. Zhao, C. Mao, X. E. Zhou, D. D. Shen, P. W. de Waal, P. Bi, C. Li, Y. Jiang, M. W. Wang, P. M. Sexton, D. Wootten, K. Melcher, Y. Zhang, H. E. Xu, Molecular Basis for Hormone Recognition and Activation of Corticotropin-Releasing Factor Receptors. *Mol Cell* **77** (2020).
38. D. Wootten, J. Simms, L. J. Miller, A. Christopoulos, P. M. Sexton, Polar transmembrane interactions drive formation of ligand-specific and signal pathway-biased family B G protein-coupled receptor conformations. *Proc Natl Acad Sci U S A* **110** (2013).
39. S. Genheden, J. W. Essex, A. G. Lee, G protein coupled receptor interactions with cholesterol deep in the membrane. *Biochim Biophys Acta Biomembr* **1859** (2017).
40. R. Guixà-González, J. L. Albasanz, I. Rodriguez-Espigares, M. Pastor, F. Sanz, M. Martí-Solano, M. Manna, H. Martinez-Seara, P. W. Hildebrand, M. Martín, J. Selent, Membrane cholesterol access into a G-protein-coupled receptor. *Nat Commun* **8** (2017).
41. G. Morra, A. M. Razavi, A. K. Menon, G. Khelashvili, Cholesterol occupies the lipid translocation pathway to block phospholipid scrambling by a G protein-coupled receptor. *Structure* **30** (2022).
42. B. I. Sejdiu, D. P. Tieleman, Lipid-Protein Interactions Are a Unique Property and Defining Feature of G Protein-Coupled Receptors. *Biophys J* **118** (2020).
43. D. L. Gater, O. Saurel, I. Iordanov, W. Liu, V. Cherezov, A. Milon, Two classes of cholesterol binding sites for the β2AR revealed by thermostability and NMR. *Biophys J* **107** (2014).
44. G. Hedger, M. S. P. Sansom, Lipid interaction sites on channels, transporters and receptors: Recent insights from molecular dynamics simulations. *Biochim Biophys Acta Biomembr* **1858** (2016).
45. J. Hu, S. J. Park, T. Walter, I. J. Orozco, G. O'Dea, X. Ye, J. Du, W. Lü, Physiological temperature drives TRPM4 ligand recognition and gating. *Nature* **630**, 509–515 (2024).
46. T. M. Cox, Eliglustat tartrate, an orally active glucocerebroside synthase inhibitor for the potential treatment of Gaucher disease and other lysosomal storage diseases. [Preprint] (2010).
47. S. Chen, L. C. Francioli, J. K. Goodrich, R. L. Collins, M. Kanai, Q. Wang, J. Alföldi, N. A. Watts, C. Vittal, L. D. Gauthier, T. Poterba, M. W. Wilson, Y. Tarasova, W. Phu, R. Grant, M. T. Yohannes, Z. Koenig, Y. Farjoun, E. Banks, S. Donnelly, S. Gabriel, N. Gupta, S. Ferriera, C. Tolonen, S. Novod, L. Bergelson, D. Roazen, V. Ruano-Rubio, M. Covarrubias, C. Llanwarne, N. Petrillo, G. Wade, T. Jeandet, R. Munshi, K. Tibbetts, M.

Abreu, C. A. Aguilar Salinas, T. Ahmad, C. M. Albert, D. Ardissino, I. M. Armean, E. G. Atkinson, G. Atzmon, J. Barnard, S. M. Baxter, L. Beaugerie, E. J. Benjamin, D. Benjamin, M. Boehnke, L. L. Bonnycastle, E. P. Bottinger, D. W. Bowden, M. J. Bown, H. Brand, S. Brant, T. Brookings, S. Bryant, S. E. Calvo, H. Campos, J. C. Chambers, J. C. Chan, K. R. Chao, S. Chapman, D. I. Chasman, R. Chisholm, J. Cho, R. Chowdhury, M. K. Chung, W. K. Chung, K. Cibulskis, B. Cohen, K. M. Connolly, A. Correa, B. B. Cummings, D. Dabelea, J. Danesh, D. Darbar, P. Darnowsky, J. Denny, R. Duggirala, J. Dupuis, P. T. Ellinor, R. Elosua, J. Emery, E. England, J. Erdmann, T. Esko, E. Evangelista, D. Fatkin, J. Florez, A. Franke, J. Fu, M. Färkkilä, K. Garimella, J. Gentry, G. Getz, D. C. Glahn, B. Glaser, S. J. Glatt, D. Goldstein, C. Gonzalez, L. Groop, S. Gudmundsson, A. Haessly, C. Haiman, I. Hall, C. L. Hanis, M. Harms, M. Hiltunen, M. M. Holi, C. M. Hultman, C. Jalas, M. Kallela, D. Kaplan, J. Kaprio, S. Kathiresan, E. E. Kenny, B.-J. Kim, Y. J. Kim, D. King, G. Kirov, J. Kooner, S. Koskinen, H. M. Krumholz, S. Kugathasan, S. H. Kwak, M. Laakso, N. Lake, T. Langsford, K. M. Laricchia, T. Lehtimäki, M. Lek, E. Lipscomb, R. J. F. Loos, W. Lu, S. A. Lubitz, T. T. Luna, R. C. W. Ma, G. M. Marcus, J. Marrugat, K. M. Mattila, S. McCarroll, M. I. McCarthy, J. L. McCauley, D. McGovern, R. McPherson, J. B. Meigs, O. Melander, A. Metspalu, D. Meyers, E. V Minikel, B. D. Mitchell, V. K. Mootha, A. Naheed, S. Nazarian, P. M. Nilsson, M. C. O'Donovan, Y. Okada, D. Ongur, L. Orozco, M. J. Owen, C. Palmer, N. D. Palmer, A. Palotie, K. S. Park, C. Pato, A. E. Pulver, D. Rader, N. Rahman, A. Reiner, A. M. Remes, D. Rhodes, S. Rich, J. D. Rioux, S. Ripatti, D. M. Roden, J. I. Rotter, N. Sahakian, D. Saleheen, V. Salomaa, A. Saltzman, N. J. Samani, K. E. Samocha, A. Sanchis-Juan, J. Scharf, M. Schleicher, H. Schunkert, S. Schönherr, E. G. Seaby, S. H. Shah, M. Shand, T. Sharpe, M. B. Shoemaker, T. Shyong, E. K. Silverman, M. Singer-Berk, P. Sklar, J. T. Smith, J. G. Smith, H. Soininen, H. Sokol, R. G. Son, J. Soto, T. Spector, C. Stevens, N. O. Stitziel, P. F. Sullivan, J. Suvisaari, E. S. Tai, K. D. Taylor, Y. Y. Teo, M. Tsuang, T. Tuomi, D. Turner, T. Tusie-Luna, E. Vartiainen, M. Vawter, L. Wang, A. Wang, J. S. Ware, H. Watkins, R. K. Weersma, B. Weisburd, M. Wessman, N. Whiffin, J. G. Wilson, R. J. Xavier, A. O'Donnell-Luria, M. Solomonson, C. Seed, A. R. Martin, M. E. Talkowski, H. L. Rehm, M. J. Daly, G. Tiao, B. M. Neale, D. G. MacArthur, K. J. Karczewski, G. A. D. Consortium, A genomic mutational constraint map using variation in 76,156 human genomes. *Nature* **625**, 92–100 (2024).

48. L. R. Kjølbye, L. Sørensen, J. Yan, N. A. Berglund, J. Ferkinghoff-Borg, C. V. Robinson, B. Schiøtt, Lipid Modulation of a Class B GPCR: Elucidating the Modulatory Role of PI(4,5)P2Lipids. *J Chem Inf Model* **62** (2022).
49. M. Damian, M. Louet, A. A. S. Gomes, C. M'Kadmi, S. Denoyelle, S. Cantel, S. Mary, P. M. Bisch, J. A. Fehrentz, L. J. Catoire, N. Floquet, J. L. Banères, Allosteric modulation of ghrelin receptor signaling by lipids. *Nat Commun* **12** (2021).
50. N. Thakur, A. P. Ray, L. Sharp, B. Jin, A. Duong, N. G. Pour, S. Obeng, A. V. Wijesekara, Z. G. Gao, C. R. McCurdy, K. A. Jacobson, E. Lyman, M. T. Eddy, Anionic phospholipids control mechanisms of GPCR-G protein recognition. *Nat Commun* **14** (2023).
51. W. Huang, M. Masureel, Q. Qu, J. Janetzko, A. Inoue, H. E. Kato, M. J. Robertson, K. C. Nguyen, J. S. Glenn, G. Skiniotis, B. K. Kobilka, Structure of the neurotensin receptor 1 in complex with β-arrestin 1. *Nature* **579** (2020).
52. A. Gomes, M. Di Michele, R. A. Roessner, M. Damian, P. M. Bisch, N. Sibille, M. Louet, J.-L. Baneres, N. Floquet, LIPIDS MODULATE THE DYNAMICS OF GPCR:β-ARRESTIN INTERACTION. *bioRxiv*, doi: 10.1101/2024.03.16.585329 (2024).
53. H. Zhang, A. Qiao, D. Yang, L. Yang, A. Dai, C. De Graaf, S. Reedtz-Runge, V. Dharmarajan, H. Zhang, G. W. Han, T. D. Grant, R. G. Sierra, U. Weierstall, G. Nelson, W. Liu, Y. Wu, L. Ma, X. Cai, G. Lin, X. Wu, Z. Geng, Y. Dong, G. Song, P. R. Griffin, J. Lau, V. Cherezov, H. Yang, M. A. Hanson, R. C. Stevens, Q. Zhao, H. Jiang, M. W. Wang, B. Wu, Structure of the full-length glucagon class B G-protein-coupled receptor. *Nature* **546** (2017).
54. A. Jazayeri, A. S. Doré, D. Lamb, H. Krishnamurthy, S. M. Southall, A. H. Baig, A. Bortolato, M. Koglin, N. J. Robertson, J. C. Errey, S. P. Andrews, I. Teobald, A. J. H. Brown, R. M. Cooke, M. Weir, F. H. Marshall, Extra-helical binding site of a glucagon receptor antagonist. *Nature* **533** (2016).
55. B. Sun, F. S. Willard, D. Feng, J. Alsina-Fernandez, Q. Chen, M. Vieth, J. D. Ho, A. D. Showalter, C. Stutsman, L. Ding, T. M. Suter, J. D. Dunbar, J. W. Carpenter, F. A. Mohammed, E. Aihara, R. A. Brown, A. B. Bueno, P. J. Emmerson, J. S. Moyers, T. S. Kobilka, M. P. Coghlan, B. K. Kobilka, K. W. Sloop, Structural determinants of dual incretin receptor agonism by tirzepatide. *Proc Natl Acad Sci U S A* **119** (2022).
56. J. K. Tiemann, M. Szczuka, L. Bouarroudj, M. Oussaren, S. Garcia, R. J. Howard, L. Delemotte, E. Lindahl, M. Baaden, K. Lindorff-Larsen, M. Chavent, P. Poulain, MDverse, shedding light on the dark matter of molecular dynamics simulations. *Elife* **12** (2024).
57. D. L. Hay, A. A. Pioszak, Receptor Activity-Modifying Proteins (RAMPs): New Insights and Roles. *Annu Rev Pharmacol Toxicol* **56** (2016).

58. A. Naglekar, A. Chattopadhyay, D. Sengupta, Palmitoylation of the Glucagon-like Peptide-1 Receptor Modulates Cholesterol Interactions at the Receptor–Lipid Microenvironment. *J Phys Chem B* **127**, 11000–11010 (2023).
59. G. Pándy-Szekeres, J. Caroli, A. Mamyrbekov, A. A. Kermani, G. M. Keseru, A. J. Kooistra, D. E. Gloriam, GPCRdb in 2023: state-specific structure models using AlphaFold2 and new ligand resources. *Nucleic Acids Res* **51** (2023).
60. A. Sali, T. L. Blundell, Comparative protein modelling by satisfaction of spatial restraints. *J Mol Biol* **234**, 779–815 (1993).
61. S. J. Park, N. Kern, T. Brown, J. Lee, W. Im, CHARMM-GUI PDB Manipulator: Various PDB Structural Modifications for Biomolecular Modeling and Simulation. *J Mol Biol* **435** (2023).
62. H. M Berman, J. Westbrook, Z. Feng, G. Gilliland, T. N Bhat, H. Weissig, I. N Shindyalov, P. E Bourne, The Protein Data Bank. *Nucleic Acids Res* **28**, 235–242 (2000).
63. P. C. Kroon, F. Grunewald, J. Barnoud, M. van Tilburg, P. C. T. Souza, T. A. Wassenaar, S. J. Marrink, Martinize2 and Vermouth: Unified Framework for Topology Generation. *Elife* **12** (2023).
64. X. Periole, M. Cavalli, S. J. Marrink, M. A. Ceruso, Combining an elastic network with a coarse-grained molecular force field: Structure, dynamics, and intermolecular recognition. *J Chem Theory Comput* **5** (2009).
65. A. L. Lomize, S. C. Todd, I. D. Pogozheva, Spatial arrangement of proteins in planar and curved membranes by PPM 3.0. *Protein Science* **31** (2022).
66. T. A. Wassenaar, H. I. Ingólfsson, R. A. Böckmann, D. P. Tieleman, S. J. Marrink, Computational lipidomics with insane: A versatile tool for generating custom membranes for molecular simulations. *J Chem Theory Comput* **11** (2015).
67. W. Song, H. Y. Yen, C. V. Robinson, M. S. P. Sansom, State-dependent Lipid Interactions with the A2a Receptor Revealed by MD Simulations Using In Vivo-Mimetic Membranes. *Structure* **27** (2019).
68. L. Borges-Araújo, P. C. T. Souza, F. Fernandes, M. N. Melo, Improved Parameterization of Phosphatidylinositide Lipid Headgroups for the Martini 3 Coarse-Grain Force Field. *J Chem Theory Comput* **18** (2022).
69. L. Borges-Araújo, A. C. Borges-Araújo, T. N. Ozturk, D. P. Ramirez-Echemendia, B. Fábián, T. S. Carpenter, S. Thallmair, J. Barnoud, H. I. Ingólfsson, G. Hummer, D. P. Tieleman, S. J. Marrink, P. C. T. Souza, M. N. Melo, Martini 3 Coarse-Grained Force Field for Cholesterol. *J Chem Theory Comput* **19** (2023).
70. Y. Qi, H. I. Ingólfsson, X. Cheng, J. Lee, S. J. Marrink, W. Im, CHARMM-GUI Martini Maker for Coarse-Grained Simulations with the Martini Force Field. *J Chem Theory Comput* **11** (2015).
71. G. Bussi, D. Donadio, M. Parrinello, Canonical sampling through velocity rescaling. *J Chem Phys* **126**, 014101 (2007).
72. M. Parrinello, Polymorphic transitions in single crystals: A new molecular dynamics method. *J Appl Phys* **52**, 7182 (1981).
73. W. Humphrey, A. Dalke, K. Schulten, VMD: visual molecular dynamics. *J Mol Graph* **14**, 33–8, 27–8 (1996).
74. Schrödinger LLC, "The PyMOL Molecular Graphics System, Version~1.8" (2015).
75. S. Kim, J. Chen, T. Cheng, A. Gindulyte, J. He, S. He, Q. Li, B. A. Shoemaker, P. A. Thiessen, B. Yu, L. Zaslavsky, J. Zhang, E. E. Bolton, PubChem 2023 update. *Nucleic Acids Res* **51** (2023).
76. D. Barneda, S. Cosulich, L. Stephens, P. Hawkins, How is the acyl chain composition of phosphoinositides created and does it matter? *Biochem Soc Trans* **47** (2019).
77. J. A. Shayman, V. Hinkovska-Galcheva, L. Shu, "Inhibitors of Glucosylceramide Synthase" in *Methods in Molecular Biology* (2023)vol. 2613.
78. A. S. Klymchenko, Fluorescent Probes for Lipid Membranes: From the Cell Surface to Organelles. *Acc Chem Res* **56** (2023).
79. M. Lucey, T. Ashik, A. Marzook, Y. Wang, J. Goulding, A. Oishi, J. Broichhagen, D. J. Hodson, J. Minnion, Y. Elani, R. Jockers, S. J. Briddon, S. R. Bloom, A. Tomas, B. Jones, Acylation of the incretin peptide exendin-4 directly impacts glucagon-like peptide-1 receptor signaling and traffickings. *Mol Pharmacol* **100** (2021).

Acknowledgments

We thank Joseph Barritt for helpful discussion.

Funding:

UKRI Future Leaders Fellowship (MR/Y01975X/1): SLR
MRC Project Grant (MR/X021467/1): AT (YM)

Wellcome Trust Discovery Award (301619/Z/23/Z): AT (AIO), SLR (GH)

Author contributions:

Conceptualization: KWC, GH, SLR, AT, JGR, JK
Methodology: KWC, LW, JK, AT
Investigation: KWC, LW, GH, SLR, YM, AIO
Visualization: KWC, LW, GH, SLR, AT, AIO, YM
Supervision: GH, AT, JGR, SLR
Writing—original draft: KWC, GH, JK, JGR, AT, SLR
Writing—review & editing: LW, AIO, JK, JGR, GH, AT, SLR

Competing interests:
Authors declare that they have no competing interests.

Data and materials availability:
All data are available in the main text or the supplementary materials. Additional data has been deposited on Zenodo

Supplementary Materials

Supplementary Materials Fig. S1-S9.